Initial Adsorption Kinetics in a Rectangular Thin Channel, and Coverage-Dependent Structural Transition Observed by Streaming Potential

CHAPTER · DECEMBER 2005

DOI: 10.1007/3-540-32658-8_3

2 AUTHORS:

Philippe Déjardin
Université de Montpellier
107 PUBLICATIONS **1,656** CITATIONS
SEE PROFILE

Elena N Vasina
27 PUBLICATIONS **201** CITATIONS
SEE PROFILE

3 Initial Adsorption Kinetics in a Rectangular Thin Channel, and Coverage-Dependent Structural Transition Observed by Streaming Potential

Philippe Déjardin, Elena N. Vasina

Abstract. One fundamental parameter contributing to the analysis of protein–solid surface interactions is the adsorption kinetic constant k_a. For a rectangular channel we give a global representation of the initial experimental adsorption constant k at distance x from the entrance channel, as a function of wall shear rate γ, through the variable $1.86\ k(x/\gamma)^{1/3}$. It is possible to visualize on a single graph the adsorption kinetic constant, the diffusion coefficient, depletion magnitude at the interface, and its thickness relative to that of the transport-limited Lévêque limit. With radiolabeled molecules (with a γ emitter like ^{125}I) and well-defined geometries, calibration does not require a known solute diffusion coefficient and is obtained from the abrupt variation of radioactivity at the buffer–protein solution change and vice-versa. Experimental data obtained for the system α-chymotrypsin/mica show that when surface coverage reaches some critical level, the streaming potential becomes almost independent of further interfacial concentration increase; this suggests an interfacial structural transition induced by interactions between adsorbed molecules. Several models based on protein–protein dipolar interactions are proposed.

3.1 Introduction

Protein adsorption at solid–liquid interfaces (Andrade 1985; Brash and Horbett 1995) is important in many fields such as hemocompatible materials (Leonard et al. 1987), diagnostic kits (Malmsten et al. 1996), enzymatic activity (Quiquampoix and Ratcliffe 1992; Servagent-Noinville et al. 2000) and environmental hazards in mineral soils (Vasina et al. 2005). Natural and artificial vessels adsorb proteins from blood. Conformational changes or reactions at interfaces can induce series of biochemical reactions. In general, this type of phenomenon must be avoided as coagulation and complement

Philippe Déjardin, Elena N. Vasina: European Membrane Institute, UMR 5635 (ENSCM-UMII-CNRS), Université Montpellier 2, CC 047, 34095 Montpellier Cedex 5, France, E-mail: philippe.dejardin@iemm.univ-montp2.fr, e.n.vasina@lboro.ac.uk

Principles and Practice
Proteins at Solid–Liquid Interfaces
Philippe Déjardin (Ed.)

systems can be activated. Application to biosensors has been proposed (Mar et al. 1999). Surface hydrophilization via polymer pretreatment can inhibit or limit these phenomena in solid-phase diagnostics (Malmsten et al. 1996), in hemodialysis hollow fibers (Yan et al. 1992) or on polymer surfaces (Lee et al. 1990). Such polymer pretreatment is generally based on copolymers that contain poly (ethylene oxide) chains (Holmberg et al. 1997; Lee et al. 1989; Nitschke et al. 2000; Price et al. 2001; Tirelli et al. 2002; Wu et al. 2000; Xu and Marchant 2000) or phosphorylcholine moeities (Huang et al. 2005; Ishihara et al. 1999a, b; Iwasaki et al. 2003; Kojima et al. 1991; Nakabayashi and Williams 2003; Nakabayashi and Iwasaki 2004; Ueda et al. 1991; Ye et al. 2005; see Chaps. 10–12). In addition, protein adsorption modifies the interfacial charge density, or the electrokinetic potential at the interface, which can be deduced from streaming potential measurements. This technique was used also to study adsorption kinetics (Ethève and Déjardin 2002; Norde and Rouwendal 1990; Zembala and Déjardin 1994).

One fundamental parameter contributing to the analysis of protein–solid surface interactions is the adsorption kinetic constant k_a, which is related to the energy barrier the protein molecule has to overcome during adsorption mechanism. Determination of the adsorption constant, however, is not straightforward: The initial adsorption process can be controlled by transport or interfacial reaction as the two extreme limits; in addition, any intermediate case can exist where both the transport and the interfacial reaction have to be taken into account and their interplay accurately described. Under well-controlled laminar flow conditions, for instance, in a channel (Fig. 1) or tube with a radius much larger than the diffusion layer thickness, the experimental adsorption kinetic constant $k(x)$ is compared to the Lévêque constant $k_{Lev}(x)$ corresponding to a fully transport-controlled process in a rectangular channel, where x is the distance from the channel entrance to the observation point. Such comparison gives a qualitative estimation of the role of transport in the overall adsorption process.

The rate of adsorption in the presence of low-concentration solutions, when the steady-state of the concentration profile $C(x, y)$ has been established, can be written as:

$$\frac{\partial \Gamma(x,t)}{\partial t} = D\left(\frac{\partial C(x,y)}{\partial y}\right)_{y=0} = k(x)\, C_b = k_a C(x,0) \tag{1}$$

where Γ is the interfacial concentration, t is the time, D is the diffusion coefficient, C_b is the bulk solution concentration; k_a is the adsorption kinetic constant at the interface, $C(x, 0)$ is the solution concentration at distance x from the channel entrance and at $y = 0$, and $k(x)$ is the kinetic constant of the overall process at x.

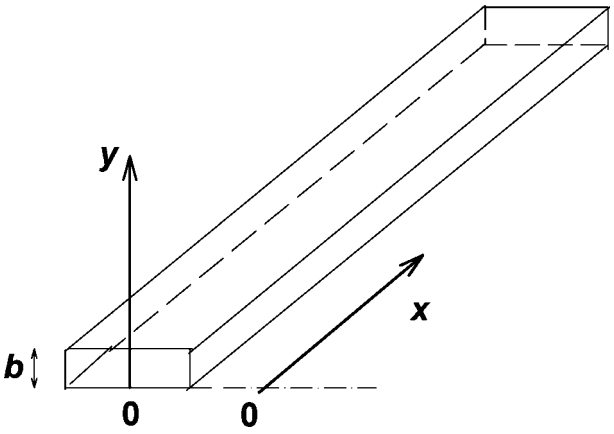

Fig. 1. Channel with rectangular section. Flow occurs in the x direction. The distance to the wall is given by y, channel height by b, and fluid velocity profile by $v(y) = \gamma y(1 - y/b)$, where γ is the wall shear rate

In case of the fully transport-controlled process ($C(x, 0) = 0$), the kinetic constant k at distance x from the entrance of the channel depends only on diffusion through the solute diffusion coefficient D and convection through the wall shear rate γ. According to Lévêque (1928) its expression is $k_{\mathrm{Lev}}(x) = 0.538\,(\mathrm{D}^2\gamma/x)^{1/3}$, a relationship that was also derived later (Levich 1962). When adsorption is controlled only by the interfacial reaction $k \approx k_{\mathrm{a}}$ and practically does not depend on x.

Figure 2 illustrates the interfacial region of depletion in solution obtained by numerical simulations. For a given solute diffusion coefficient, the higher the adsorption kinetic constant, k_{a}, the larger the interfacial depletion, and the larger the distance from the channel entrance, the larger the thickness, δ, of the depletion layer and the depletion magnitude at the surface. Hence the crossover length L_{co} (Eq. 5c) was introduced in the complete treatment (Déjardin et al. 1994), contrary to the simpler case of the rotating disk where δ is constant (Coltrin and Mitchell 2003; Levich 1962). We define the depletion $d(x)$ at the interface:

$$d(x) = 1 - \frac{C(x, 0)}{C_{\mathrm{b}}} \tag{2}$$

As the steady-state adsorption rate is related to the slope of $C(x, y)$ at the wall (Eq. 1):

$$\frac{\partial\, \Gamma(x, t)}{\partial\, t} = D\frac{C_{\mathrm{b}} - C(x, 0)}{\delta(x)} = k(x)\, C_{\mathrm{b}} = k_{\mathrm{a}}\, C(x, 0) \tag{3}$$

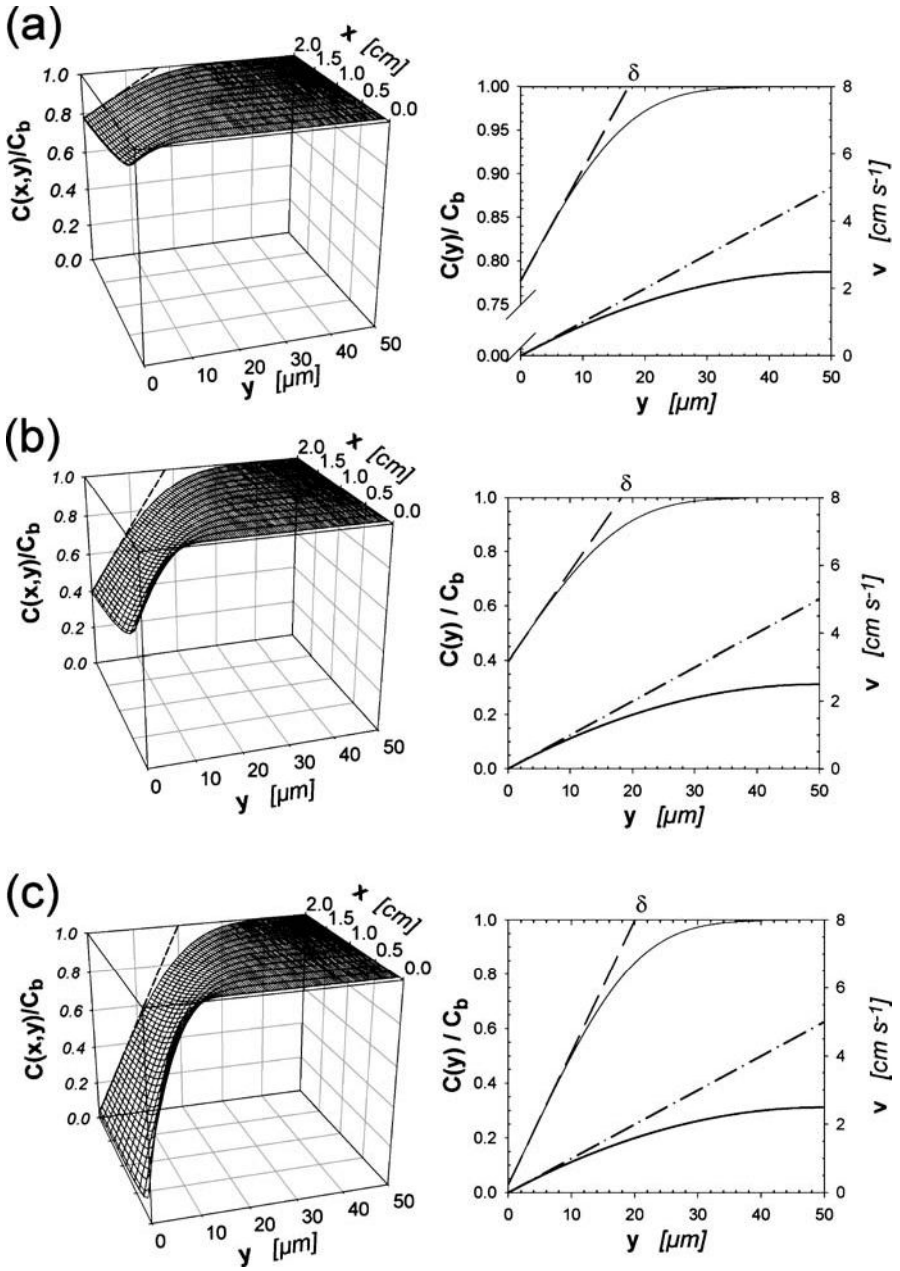

Fig. 2. Stationary concentration profiles normalized to the bulk concentration C_b, for $D = 6.0\times10^{-7}$ cm^2 s^{-1}, and wall shear rate 1,000 s^{-1}. Channel height is 100 μm. *Left* Three-dimensional graph $C(x, y)$ from the entrance to distance $x = 2$ cm. *Right* Concentration profile at $x = 2$ cm, with the tangent to the profile at the wall (*dashed line*, left scale), and parabolic velocity profile with the tangent at the wall (*dash-dotted line*, right axis). **a** $k_a = 1.0\times10^{-4}$ cm s^{-1}; **b** $k_a = 5.0\times10^{-4}$ cm s^{-1}; **c** $k_a = 1.0\times10^{-2}$ cm s^{-1}

we obtain:

$$k(x) = k_a\,[1 - d(x)] = D\frac{d(x)}{\delta(x)}\,. \tag{4}$$

The Lévêque limit where depletion is complete corresponds to $d \to 1$, $k_{Lev}(x) = D/\delta_{Lev}(x)$ and $\delta_{Lev}(x) = 1.859(Dx/\gamma)^{1/3}$. When approaching this limit, $k(x) \ll k_a$, while for the opposite one of a negligible depletion $k(x) \to k_a$.

The Damköhler number, $Da = k_a/<v>$, where $<v>$ is the average velocity of the fluid, is often used as a criterion to separate the domains of control by the interfacial reaction ($Da \ll 1$) and by transport ($Da \gg 1$), especially in studies concerning porous media (Adler and Thovert 1998). There is a direct connection between the ratio k_a/k_{Lev} and this number. The difference originates from the introduction of the diffusion coefficient. Other expressions of Da are used that also take it into account (Bizzi et al. 2002; Coltrin and Mitchell 2003) for gas phases: $Da = k_a/(D/\delta)$, where δ is the diffusion layer thickness. In the present problem, we can define a Damköhler number $Da(x) = k_a/k_{Lev}(x)$, with $k_{Lev}(x) = D/\delta_{Lev}(x)$.

As summarized earlier (Docoslis et al. 1999), the experimental determination of the adsorption kinetic constant k_a has three major sources of difficulties: (1) mass transport, easier to take into account with the simple geometries of rectangular channels or circular tubes, (2) steric hindrance at the interface, which can be limited by using low-concentration solutions, and (3) determination of low interfacial concentration, which requires very sensitive techniques, usually using radioactive or fluorescently labeled molecules like in the total internal reflection fluorescence (TIRF) technique (Britt et al. 1998; Buijs et al. 1998; Kelly and Santore 1995; Malmsten et al. 1996; Rebar and Santore 1996; Robeson and Tilton 1996; Wertz and Santore 2002). Sophisticated optical methods such as surface plasmon resonance (SPR; Mar et al. 1999) and optical waveguide lightmode spectroscopy (OWLS; Calonder and Van Tassel 2001; Hook et al. 2002; Ramsden et al. 1995; Chaps. 1–2) provide the means to measure low interfacial concentrations without labeled molecules.

The following data treatment can be useful for the SPR, reflectometry, ellipsometry, and OWLS techniques if the experimental flow cells have rectangular channel geometries. For instance, in OWLS experiments, a chamber tightened with an O-ring joint is not adapted to the present formulation as the channel width varies continuously and strongly near the inlet, which leads to a nonconstant wall shear rate. In this case the Lévêque limit formula is no longer applicable. The cell has to be adapted (Chap. 1) to achieve a constant width. Moreover, the height of the channel should be large enough to provide a linear velocity profile in the depletion layer, which is assumed in the Lévêque derivation, and its extension to finite k_a (Déjardin et al. 1994).

For example, in Fig. 2 the channel height of 100 μm is too small to fulfill the criterion when $D = 6.0\times10^{-7}$ cm^2 s^{-1} and $\gamma = 1{,}000\,\mathrm{s}^{-1}$. Another technique is the impinging jet on a flat substrate, which was also used in combination with TIRF to study the deposition of latex particles (Göransson and Trägardh 2000). Here we do not consider this kind of geometry.

In the first part of the present work we recall derivation of the simple accurate approximations, providing an easy way to treat quantitative data; thus, one can deduce the protein diffusion coefficient D and protein interfacial adsorption kinetic constant k_a from experimental initial constant k as a function of the variable $(k/k_{Lev})D^{2/3}$, where $k_{Lev}/D^{2/3}$ does not depend on D.

In the second part, we present the variation of the interfacial potential as a function of surface coverage and suggest the possible importance of protein–protein dipolar attractive interactions to create domains with an antiferroelectric order at high coverage.

3.2 The Initial Adsorption Constant and its Limit Expressions

3.2.1 The Local Initial Adsorption Constant $k(x)$, its Limit Expressions and Approximation

Full Solution and Limit Expressions

Let us recall that the general expression (Dejardin et al. 1994) for the constant $k(x)$ at distance x from the channel entrance as a function of k_a and k_{Lev} is not easily accessible for the determination of k_a.

$$k(x) = k_a g(X)\ , \tag{5a}$$

with

$$X = \frac{x}{L_{co}} \tag{5b}$$

where

$$L_{co} = 3\left(\frac{\Gamma'(2/3)}{\Gamma'(1/3)}\right)^3 \frac{D^2\gamma}{k_a^3} \tag{5c}$$

and

$$g(X) = \mathrm{e}^{-X} + G(2/3, X) - G(1/3, X) \tag{5d}$$

with

$$G(n,x) = \frac{1}{\Gamma'(n)} e^{-X} \int_0^X z^{n-1} e^z dz \tag{5e}$$

$\Gamma'(n)$ is the usual gamma function (Abramovitz and Stegun 1972). The prime is added to avoid confusion with Γ used for the interfacial concentration.

It is preferable to have k_a as a function of experimental $k(x)$. It has been shown that rather good approximations of the general solution can be obtained at the two limits of the controls by transport and the interfacial reaction (Dejardin et al. 1994). These involve the inverse of the kinetic constants and, in fact, lead directly to the interpretation of the total resistance (time) of the adsorption process as being the sum of one resistance due to the transport and the other resistance due to the interfacial reaction. Close to the conditions of the transport-controlled process,

$$k^{-1} = k_{Lev}^{-1} + 0.684 k_a^{-1} , \tag{6a}$$

while close to the conditions of the control by interfacial reaction

$$k^{-1} = 0.827 k_{Lev}^{-1} + k_a^{-1} \tag{6b}$$

Both expressions are similar to the simplest approximation, which considers no coupling between transport and the interfacial reaction:

$$k^{-1} = k_a^{-1} + k_{Lev}^{-1} \tag{7}$$

Equation 7 can be also obtained by assuming that the thickness of the diffusion layer (when $C(x, y = 0) = 0$, Lévêque model) is unaltered whatever the finite value of k_a, say whatever the nonzero steady-state value of the volume concentration near the interface. Equation 7 corresponds to the work (Bowen and Epstein 1979) and matches Eq. 2.45 of Bowen et al. (1976).

Approximation of $k(x)/k_a$ as a function of $k(x)/k_{Lev}(x)$

If the linear approximations given in Eq. 6a and b are valid at to the two limits can be useful in practice, as it is easy to deduce k_a from $k(x)$ and $k_{Lev}(x)$, they do not describe the entire domain as does the general expression (which writes k as a function of k_a, not the reverse). Recently we have proposed (Déjardin and Vasina 2004) to approximate the general expression in Eq. 5a by the function $y = f(u)$, where $y = k/k_a$ and $u = k/k_{Lev}$:

$$f(u) = \frac{(u-1)(au-1)}{(bu+1)} \tag{8}$$

with $a = 0.451707$ and $b = -0.624713$, to satisfy the two limits of Eq. 6a,b. The greatest relative variation between Eq. 8 and the complete calculation

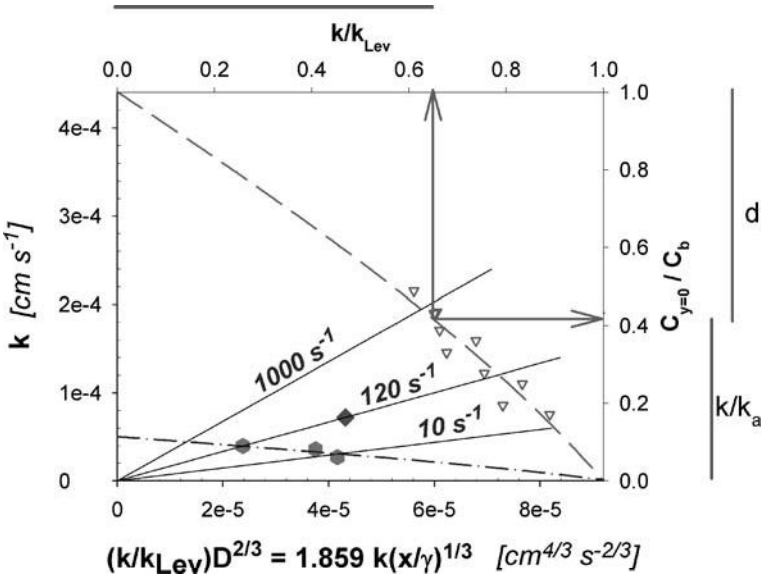

Fig. 3. Adsorption of α-chymotrypsin (∇, *dashed line*, 10^{-2} M Tris; pH 8.6) onto mica. The normalization of the scales to the intercepts k_a and $D^{2/3}$ illustrates the magnitude of the depletion at the interface ($C_{y=0}/C_b$; right axis), where y is the distance to the interface, and the departure from the fully transport-limited process (k/k_{Lev}; top axis). For measurements performed at the same distance x, the experimental points corresponding to one given wall shear rate are positioned on a *straight line* passing through the origin. An example is provided with the points corresponding to experiments in 10^{-2} M (∇), 0.2 M ($\blacklozenge$) and 0.5 M ($\blacklozenge$ *dash-dotted line*) Tris, pH 8.6

is 1% around $u = 0.8$. Let us note that $k(x)/k_a = C(x,0)/C_b$, so the ordinate illustrates the depletion in solution at the interface, while $u = k/k_{Lev}$ estimates contribution of the transport. Figure 3 shows an example of these two items.

Equation 8 can be transformed into a two-parameter fit (D and k_a) to experimental $k(x,\gamma)$ as a function of $u' = k(x/\gamma)^{1/3}/0.538 = uD^{2/3}$, which does not require the knowledge of D.

$$k = \frac{k_a}{D^{2/3}} \frac{(u' - D^{2/3})(au' - D^{2/3})}{bu' + D^{2/3}} \tag{9}$$

In such a representation, the intercept of the fit with the ordinate axis gives k_a, while the intercept with the abscissa axis gives $D^{2/3}$ (see Fig. 3). Figure 4 illustrates the magnitude of error in the adsorption kinetic constant k_a and diffusion coefficient D that can occur when using Eq. 7. Equation 7 corresponds there to the straight line $k = k_a(1 - u'/D^{2/3})$.

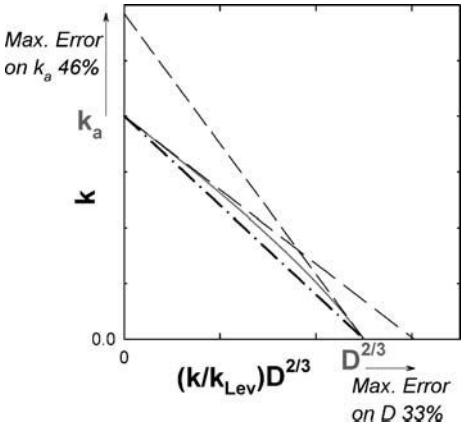

Fig. 4. Illustration of the maximum (*Max.*) error on adsorption constant k_a and diffusion coefficient D when neglecting any coupling between transport and interfacial reaction (*straight dash-dotted line*; Eq. 7 in text), compared to exact solution (*full curved line*). The *dashed lines* demonstrate linear approximations at the two extreme limits

3.2.2 The Mean Adsorption Constant, its Limit Expressions and Approximation

Mean <*k*> Over the Full Length of the Channel

In some cases it is necessary to find the average adsorption constant over the full sample length where laminar convection occurs. When the process is fully transport-controlled, the integration of the local Lévêque equation over the channel length L leads to $<k_{Lev}> = 0.808(D^2\gamma/L)^{1/3}$. When the contribution of the interfacial reaction is taken into account, the mean kinetic constant <*k*> over the channel length L is given by (Valette et al. 1999):

$$<k> = \frac{k_a}{\Lambda}\int_0^{\Lambda} g(X)\mathrm{d}X \tag{10a}$$

where:

$$\Lambda = \frac{L}{L_{co}} = \left[\frac{3}{2\Gamma'(2/3)}\frac{k_a}{<k_{Lev}>}\right]^3 \tag{10b}$$

Hence:

$$<k> = \frac{k_a}{\Lambda}\left(1 + \frac{3\Lambda^{2/3}}{2\Gamma'(2/3)} - \frac{3\Lambda^{1/3}}{\Gamma'(1/3)} - g(\Lambda)\right) \tag{10c}$$

Close to the conditions of transport-controlled process, we have:

$$<k>^{-1} \approx <k_{\mathrm{Lev}}>^{-1} + 0.913 k_{\mathrm{a}}^{-1} \tag{10d}$$

while close to the conditions of control by the interfacial reaction

$$<k>^{-1} \approx k_{\mathrm{a}}^{-1} + 0.930 <k_{\mathrm{Lev}}>^{-1} \tag{10e}$$

with the total resistance being the sum of the two resistances (one due to the transport and the other one due to the interfacial reaction).

As the numerical coefficients in both linear approximations are close to 1, the simple approximation

$$<k>^{-1} \approx k_{\mathrm{a}}^{-1} + <k_{\mathrm{Lev}}>^{-1} \tag{11}$$

is rather good for the whole range of k_{a}. The same route as that for the local adsorption constant led to the following approximation of $<k>/k_{\mathrm{a}}$ as a function of $U = <k>/< k_{\mathrm{Lev}}>$:

$$F(U) = \frac{(U-1)(AU-1)}{(BU+1)} \tag{12}$$

where $A = 0.203127$ and $B = -0.272759$, to satisfy Eqs. 10d–e. The greatest relative variation between Eq. 12 and the complete calculation is 0.03% around $U = 0.8$. It can be used in the form $<k> = k_{\mathrm{a}} F(U)$ for a two-parameter fit (D and k_{a}) to the experimental value of $<k>$ as a function of $U' = <k>(L/\gamma)^{1/3}/0.808 = UD^{2/3}$.

$$\langle k \rangle = \frac{k_{\mathrm{a}}}{D^{2/3}} \frac{(U' - D^{2/3})(AU' - D^{2/3})}{BU' + D^{2/3}} \tag{13}$$

Mean [*k*] Over a Restricted Length

In experiments, the adsorption kinetics is always integrated over some length Δx of the channel, between $x - \Delta x/2$ and $x + \Delta x/2$. We shall estimate the influence of Δx on the numerical coefficients a and b in Eqs. 8 or 9.

Referring to Eq. 8, the variable $u = k(x)/k_{\mathrm{Lev}}(x)$ becomes $u^* = [k]/[k_{\mathrm{Lev}}]$, where the star superscript and the brackets mean that the average is taken between $x_1 = x - \Delta x/2$ and $x_2 = x + \Delta x/2$. $[k]$ is the actual measured average kinetic constant, which was assumed to be $k(x)$ in Eq. 8, and $[k_{\mathrm{Lev}}] = \Delta x^{-1}(x_2 <k_{\mathrm{Lev}}>_2 - x_1 <k_{\mathrm{Lev}}>_1)$. $<k_{\mathrm{Lev}}>_i$ is the mean value of the Lévêque constant between $x = 0$ and $x = x_i$.

We adopt the same procedure looking for two limit expressions for a transport-limited process and interfacial reaction control (see Appendix). For small values of $\varepsilon = \Delta x/x$ we obtain:

$$a \approx a_0 \left(1 + 0.078\,\varepsilon^2\right) \; ; \quad b \approx b_0 \left(1 + 0.044\,\varepsilon^2\right) \tag{14}$$

where a_0 and b_0 are the values of the numerical coefficients determined in Eq. 8, which corresponds to $\Delta x \to 0$.

3.2.3
Experimental Results and Discussion

A flow cell of adequate dimensions $4 \times 11 \times 1$ cm (to be inserted in a detector of gamma radioactivity) consisted of two polymethylmethacrylate plates, between which were pressed two mica plates separated by a spacer. A top view of the cell is provided in Fig. 5. The data acquisition was performed using the same kind of procedure as for capillary geometry (Boumaza et al. 1992; Le and Déjardin 1998). For a detection window of width w and a channel height h, the radioactivity jump at the arrival of radiolabeled protein solution is $A_v \sim whC_b$, while the surface radioactivity on the two faces (mica plates) is $A_s \sim 2w\Gamma$. Therefore $\Gamma(t) = (h/2)C_b A_s(t)/A_v$ and $k(t) = (h/2)(dA_s/dt)/A_v$.

Recently we studied (Vasina and Déjardin 2004) the adsorption of α-chymotrypsin onto mica at different concentrations of Tris buffer at pH 8.6. Examples of the adsorption kinetics data are given in Fig. 6. The initial adsorption rate is linear with a protein solution concentration in the range considered (Fig. 7).

In Fig. 3 some of our results emphasizing the peculiarities of the representation given by Eq. 9 are plotted. The scanning of adsorption with

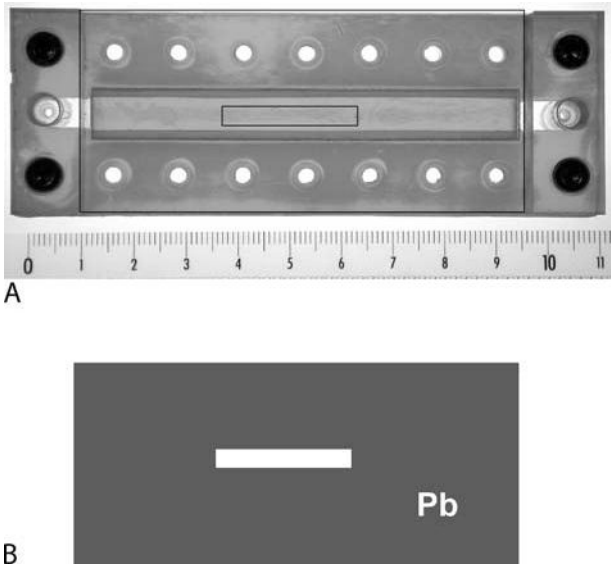

Fig. 5. (**A**) Top view of the experimental cell showing the mica sheets constituting the two faces of the channel (scale in centimeters). Measurement of adsorption concerns only the central part of the cell, using appropriate lead shields (**B**). The cell is inserted in a γ-radioactivity detector

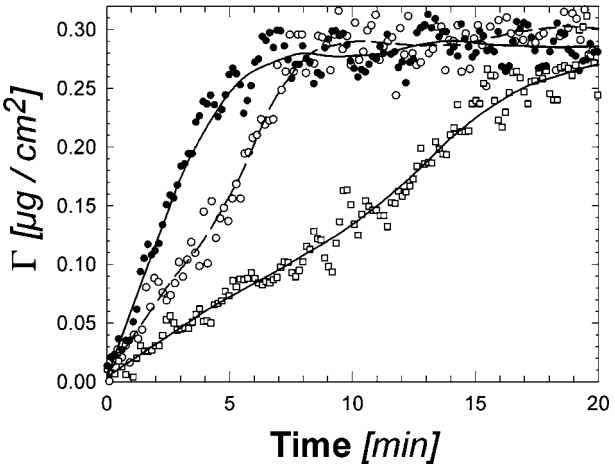

Fig. 6. Experimental data of adsorption kinetics of α-chymotrypsin on mica recorded for wall shear rate 120 s^{-1} and different bulk α-chymotrypsin concentrations, C_b: 10 μg ml^{-1} (●); 5 μg ml^{-1} (○); 2.5 μg ml^{-1} (□)

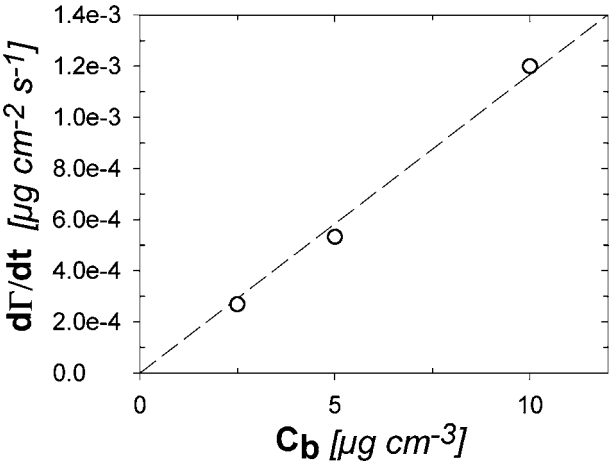

Fig. 7. Initial adsorption rate of α-chymotrypsin on mica as a function of solution concentration C_b at pH 8.6, Tris buffer (concentration 10^{-2} M). Mean slope (*dashed line*) $k \approx 1.2 \times 10^{-4}$ cm s^{-1}

convection is viewed as straight lines passing through the origin with their slope increasing with wall shear rate γ as 0.538 $(\gamma/x)^{1/3}$. The application of Eq. 9 to the adsorption of α-chymotrypsin onto mica in the rectangular channel provides two parameters: the diffusion coefficient D and the adsorption kinetic constant k_a (for instance, in 10^{-2} M Tris buffer, pH 8.6: $D = 8.8 \pm 0.7 \times 10^{-7}$ cm^2 s^{-1} and $k_a = 4.4 \pm 0.5 \times 10^{-4}$ cm s^{-1}). The two-parameter fit was performed using SigmaPlot®.

The depletion (Eq. 2) with its complement to unity, say $k(x, y)/k_a$ or $C(x, 0, y)/C_b$, is directly visualized in Fig. 3. Moreover, given the curvature of the function $k(u')$, the thickness of the depletion layer is always smaller than that of the Lévêque model, as $k(x, y) = Dd(x, y)/\delta(x, y)$ with $d(x, y) = 1$ in the Lévêque limit, therefore $\delta(x, y)/\delta_{Lev}(x, y) = d(x, y)/[k(x, y)/k_{Lev}(x, y)]$. Both terms of the ratio are noted in Fig. 3.

In our experiments, the detection occurs between 2.5 and 5.5 cm from the channel entrance, therefore $\varepsilon = 0.75$. Taking into account this range of integration (Eqs. 9 and 14), we obtain for Tris buffer 10^{-2} M at pH 8.6, corrections of –1% for the protein diffusion coefficient D and +6% for its adsorption kinetic constant k_a.

When comparing the present treatment to other works in the literature, we should mention that we do not assume any value for the protein diffusion coefficient. The calibration is provided by the increase in radioactivity when the radiolabeled protein solution arrives in a channel of known geometry or by its drop when the radiolabeled solution is replaced by buffer. We do not assume any Lévêque regime with a known diffusion coefficient, as is sometimes assumed in fluorescence (TIRF) experiments (Wertz and Santore 1999, 2002).

3.3 The Structural Transition with Increasing Interfacial Concentration

As can be seen in Fig. 6, the adsorption rate slightly increases at about half the maximum interfacial concentration. Such an increase could be the signature of a structural change at the interface. It was recognized for many years that protein crowding at the interface leads to profound changes there because of the increasing probability of the protein–protein interactions (Andrade 1985). In the present case, such a change in the adsorption rate could also be caused by the conditions of flow in the channel, associated with the early saturation of the surface upward of the point of examination. Simulations suggest, however, that this hypothesis should be rejected, as it would require an adsorption constant much higher than that deduced from the previous analysis (Vasina and Dejardin 2004). To describe the conformational changes (see Chap. 6) and/or orientation, many models can be proposed, among them the side-on/end-on process, the reverse process, and the spreading of the (soft) protein on the surface. Techniques like neutron reflectivity (Su et al. 1998), ellipsometry (Bae et al. 2005; Cuypers et al. 1978; McClellan and Franses 2005; Poksinski and Arwin 2004; Seitz et al. 2005; Werner et al. 1999), and scanning angle reflectometry (Ladam et al. 2002; Schaaf and Déjardin 1988) are able to provide information about

the orientation of an ellipsoid-modeled molecule. Circular dichroism and differential scanning calorimetry are also useful in the study of the protein conformations (Giacomelli and Norde 2001; Norde and Zoungrana 1998; Vermeer and Norde 2000; Vermeer et al. 2001; Voegel et al. 1987; Zoungrana et al. 1997). Infrared attenuated total reflection (Noinville et al. 2002a,b, 2003) provides data about possible changes in the tertiary structure (see Chap. 6).

The TIRF technique was refined to take into account the dependence on the emission properties of the fluorophore with its ionization state or with the electric potential (Daly et al. 2003; Robeson and Tilton 1996). If the ionic strength is chosen in such a way that the interfacial electric potential varies over a distance comparable to the protein size, then the signal will be dependent upon the orientation of the molecule. Indeed the interfacial transition is easily observed and is concomitant with the change in kinetic regime.

3.3.1 Observation by Streaming Potential

Measurement of streaming current (Daly et al. 2003) and streaming potential (Ethève and Dejardin 2002; Vasina and Dejardin 2004) during adsorption can be useful to obtain information on the orientation of molecules at interfaces. The variation of streaming potential with protein interfacial concentration exhibits a change at some critical concentration for the α-chymotrypsin/mica system at pH 8.6 in 10^{-2} M Tris (Fig. 8). The variation in zeta potential was deduced from the streaming potential, E_s, as a function of time at a defined pressure differential, ΔP, via the classical Smoluchowski relationship (Hunter 1981), with $\Delta E_s = E_s - E_{s0}$, where E_{s0} is the asymmetry potential,

$$\varsigma = \frac{\Delta E_s}{\Delta P} \frac{\eta \lambda_0}{\varepsilon_0 \varepsilon_r} \tag{15}$$

where λ_0 is the electrolyte solution conductivity, η is the solution viscosity, ε_0 is the vacuum dielectric permittivity and ε_r is the relative permittivity.

The quantitative analysis of the data, however, is not simple as initially, when transport is important, the interfacial concentration is not uniform. Indeed, the Smoluchowski relationship assumes a uniform charge density along the channel walls. For another system – lysozyme/silica capillary; pH 7.4, 10^{-2} M phosphate buffer (Ethève and Dejardin 2002) – we observed the same kind of variation and assumed that the streaming potential resulted from the mean charge density along the capillary and estimated by numerical simulations the average interfacial concentration. This did not

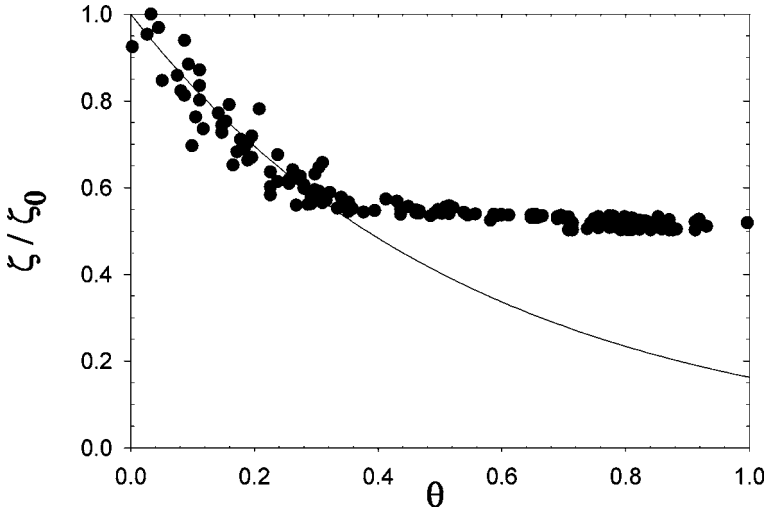

Fig. 8. Variation of the ζ potential, relative to the initial ζ_0 potential (–95 mV) of the bare mica, as a function of α-chymotrypsin interfacial concentration. Solution concentration C_b = 2.5 μg ml^{-1} in Tris 10^{-2} M, pH 8.6. Wall shear rate 120 s^{-1}. The *full line* represents the expected variation, based on the behavior at small θ, for particles bearing only one type of charge

lead to any dramatic changes in the observation of the transition. After the transition, local and average concentrations become much closer.

When comparing to similar works with random deposition of uniformly charged particles (Zembala and Adamczyk 2000) where such transition was not observed, it was concluded that the transition could be the result of the peculiar nature of the proteins. Contrary to the particles, proteins bear the two types of charge, positive and negative. Moreover, the charge distribution on the protein surface is not uniform. Let us analyze the present system along the same lines as the ones used for particles. As a first approximation, α-chymotrypsin can be assumed globally neutral because its isoelectric point is 8.2. For particles, the variation of ζ/ζ_0 with coverage was described as obeying a sum of an exponential function and a linear one (Zembala and Adamczyk 2000).

$$\frac{\zeta}{\zeta_0} = e(C_i^0 \vartheta) + \frac{\zeta_p}{\zeta_0} C_p^0 \vartheta \tag{16a}$$

where ζ_0 and ζ_p are the potentials of the bare surface and uniformly charged particle, respectively, in the presence of buffer. After additional control experiments, another expression was proposed (Zembala 2004):

$$\frac{\zeta}{\zeta_0} = e(C_i^0 \vartheta) + \frac{\zeta_p}{\zeta_0} \left[1 - e(-C_p^0 \vartheta)\right] \tag{16b}$$

When the particle radius r is much larger than the Debye length κ^{-1}, then $C_i^0 = -10.21$ and $C_p^0 = 6.51$. The dependence of those coefficients on rκ has been established (Zembala et al. 2001). As the dimensions of α-chymotrypsin are $5.1 \times 4 \times 4\,\mathrm{nm}^3$, with $r = 2{-}2.5\,\mathrm{nm}$ and $\kappa^{-1} = 6.3\,\mathrm{nm}$, we have $r\kappa = 0.3 - 0.4$, thus $C_i^0 \approx -4.5{-}5$. As the net protein charge is almost zero, according to the model, the variation of ζ/ζ_0 should follow an exponential decay, $\exp(-C_i^0\theta)$, corresponding to the flow attenuation or substrate charge screening by the deposited neutral protein particles. We found the constant 1.8 instead of 4.5 (Fig. 8). The passage from local to mean coverage by simulations leads to the slightly lower value of 1.7. The smaller decrease in ζ/ζ_0 with coverage, compared to what should be expected from the model, may have two explanations: the distribution of charges on the protein surface and/or the nonrandom adsorption (Dabros and van de Ven 1993). It is clear, however, that whatever the mechanism, proteins and homogeneously charged particles have different qualitative behaviors at high coverage. The reason is probably the protein–protein interaction associated with the mobility of proteins on the surface. As α-chymotrypsin possesses a high dipole moment (483 D; Antosiewicz and Porschke 1989), the reasonable model of parallel dipoles at low ionic strength and low coverage, based on the ionic interaction between the mica and the protein, would lead at high coverage to a strong repulsion component between parallel dipoles, when the distance between like charges become shorter. As experiments show that the maximum interfacial concentration for proteins, and especially here for α-chymotrypsin, is generally near the full close-packed monolayer, some specific mechanism should occur.

3.3.2 Different Models

Figure 9 illustrates the two models of rearrangements of the dipoles roughly normal or parallel to the surface to obtain an attractive component between adsorbed proteins. We proposed the model of the ferroelectric-antiferroelectric arrangement normal to the surface to explain the change in variation of the ζ potential (Vasina and Dejardin 2004; Fig. 9, left). Saving almost the same orientation of the proteins with respect to the surface (Robeson and Tilton 1996), cooperative clustering could appear also by dipolar interactions in the direction parallel to the surface (Fig. 9, right). The complete analysis would, however, require a careful description of the balance between attractive and repulsive electrostatic components, probably in connection with the local concentration of small ions. Such ferroelectric to antiferroelectric order transition was already considered for

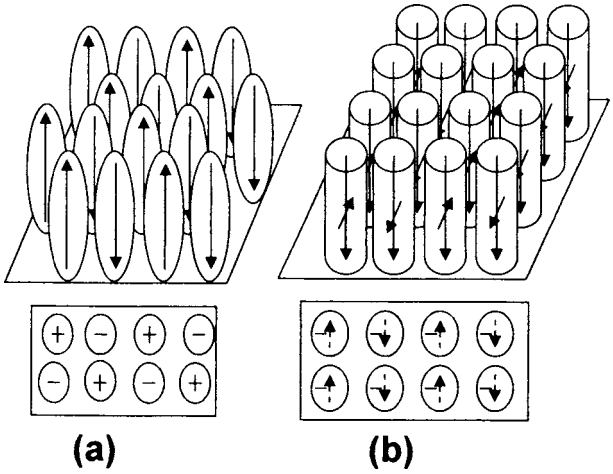

Fig. 9. Schematic representation of possible ordered domains at the interface, with a top view of the charge repartitions. **a** Alternate orientation of the dipoles normal to the surface for intermolecular attraction, but with a repulsive component in front of the surface. **b** Alternate orientation of the dipoles parallel to the surface for intermolecular attraction, but with a repulsive intermolecular component between the likely oriented dipoles normal to the surface. Ellipsoid or cylinder representation is arbitrary

small dipolar molecules like carbon monoxide and halogenated methane (Burns and Dennison 1998; Burns et al. 2004).

Recently, it was shown by TIRF and streaming-current measurements on the lysozyme/silica system at high wall shear rates that the TIRF overshoot did not correspond to any particular event in the interfacial potential (Daly et al. 2003). Therefore, it appears that the concomitance of the changes in kinetic regime and interfacial potential is not always the rule. One important phenomenon behind the process is surface diffusion, which has to be taken into account. Different kinds of behavior are probably linked to the relative rate of arrival of molecules compared to their surface diffusion rate (see Chap. 2).

3.4 Conclusion

We proposed simple relationships in the channel geometry to describe the passage from a fully transport-controlled process to an interface-controlled one when increasing convection (say wall shear rate γ) for a study at some distance x from the entrance, as well as for the average value over the full or partial length of the channel (or wall). The experimental data of the initial experimental kinetic constant $k(x, \gamma)$ are plotted as a function of

$(k/k_{\mathrm{Lev}})D^{2/3}$, where k_{Lev} is the Lévêque limit and D the diffusion coefficient. The adsorption kinetic constant k_{a} and the protein diffusion coefficient to power 2/3 can be easily determined as the intercepts of the fit curve with the ordinate and abscissa axes, respectively. The normalizations of ordinates and abscissae to the intercepts provide directly the magnitude of the depletion in the liquid phase at the interface, and the relative evaluation to the transport-limited process. An example is given for the system α-chymotrypsin/mica at pH 8.6.

The variation of ζ potential as a function of surface coverage exhibits a change of regime, this suggests a new arrangement of adsorbed protein molecules above a threshold of surface occupation. The possibility of dipolar attractive interactions between the proteins is considered to create domains with an antiferroelectric order at high coverage.

Acknowledgements. We are grateful to R. Souard and P. Montels (EMI) for manufacturing the flow cell, and to D. Cot (EMI) for the photo. This work was supported by "Programme Ecologie Quantitative" of the French Ministry of Research, and performed within the framework of collaboration between Centre National de la Recherché Scientifique (France) and Kazan State University (Russia), project 12889.

Appendix

We study the influence of the length of examination Δx around the average mean distance to the channel entrance x, through the parameter $\varepsilon = \Delta x/x$, on the numerical parameters a and b determined in Eq. 8. The two local limit expressions, valid near the control by the interfacial reaction (Eq. 6b) or by transport (Eq. 6a), can be written as $k^{-1}(x) = c_{\mathrm{a}}k_{\mathrm{a}}^{-1} + c_{\mathrm{L}}k_{\mathrm{Lev}}^{-1}(x)$, where c_{a} and c_{L} are numerical coefficients (Dejardin et al. 1994; Dejardin and Vasina 2004). In what follows, the average between $x_1 = x - \Delta x/2$ and $x_2 = x + \Delta x/2$, is indicated by the use of brackets [].

1. $k \approx k_{\mathrm{a}} \ll k_{\mathrm{Lev}}$; $c_{\mathrm{a}} = 1.0$; $c_{\mathrm{L}} = 0.827$

$$k(x) \approx k_{\mathrm{a}}\left(1 - c_{\mathrm{L}}\frac{k_{\mathrm{a}}}{k_{\mathrm{Lev}}}\right) \tag{A1a}$$

or

$$[k(x)]^{-1} = k_{\mathrm{a}}^{-1} + c_{\mathrm{L}}\left[k_{\mathrm{Lev}}^{-1}(x)\right] \tag{A1b}$$

2. $k \approx k_{\mathrm{Lev}} \ll k_{\mathrm{a}}$; $c_{\mathrm{L}} = 1.0$; $c_{\mathrm{a}} = 0.684$

$$k(x) \approx k_{\mathrm{Lev}}(x)\left(1 - c_{\mathrm{a}}\frac{k_{\mathrm{Lev}}(x)}{k_{\mathrm{a}}}\right) \tag{A2a}$$

or

$$[k(x)]^{-1} \approx [k_{\mathrm{Lev}}(x)]^{-1} + c_a\, k_{\mathrm{a}}^{-1} \frac{\left[k_{\mathrm{Lev}}^2(x)\right]}{[k_{\mathrm{Lev}}(x)]^2} \tag{A2b}$$

We are looking for an expression of $[k\ (x)]/k_{\mathrm{a}}$ as a function of $u^* = [k(x)]/[k_{\mathrm{Lev}}(x)]$. The relationships A1 and A2 are written as:

$$[k(x)]/k_{\mathrm{a}} = 1 - c_{\mathrm{L}}[k(x)][k_{\mathrm{Lev}}^{-1}] \tag{A3}$$

$$[k(x)]/k_{\mathrm{a}} = c_{\mathrm{a}}^{-1}([k_{\mathrm{Lev}}(x)]^2/[k_{\mathrm{Lev}}^2(x)])(1 - u^*) \tag{A4}$$

with

$$[k_{\mathrm{Lev}}^{-1}(x)] \approx [k_{\mathrm{Lev}}(x)]^{-1} \left(1 + \frac{1}{108}\varepsilon^2\right) \tag{A5}$$

and

$$\frac{[k_{\mathrm{Lev}}^2(x)]}{[k_{\mathrm{Lev}}(x)]^2} \approx 1 + \frac{1}{108}\varepsilon^2 \tag{A6}$$

The final relationship:

$$[k(x)]/k_{\mathrm{a}} = 1 - c_{\mathrm{L}}(1 + \varepsilon^2/108)u^* \tag{A7}$$

$$[k(x)]/k_{\mathrm{a}} = c_{\mathrm{a}}^{-1}(1 + \varepsilon^2/108)(1 - u^*) \tag{A8}$$

must be the limits of the function $\phi_\varepsilon(u^*)$ as $u^* \to 0$ and $u^* \to 1$, respectively:

$$\phi_\varepsilon(u^*) = \frac{\left(u^* - 1\right)\left(a_\varepsilon\, u^* - 1\right)}{\left(b_\varepsilon\, u^* + 1\right)} \tag{A9}$$

We found for the first terms in powers of ε (for $\varepsilon < 1$) $a_\varepsilon = a_0(1 + 0.078\varepsilon^2)$ and $b_\varepsilon = b_0(1 + 0.044\varepsilon^2)$

References

Abramovitz M, Stegun IA (1972) Handbook of Mathematical Functions. Dover Publications, New York, p 255

Adler PM, Thovert J-F (1998) Real porous media: local geometry and macroscopic properties. Appl Mech Rev 51:537–585

Andrade J (1985) Surface and Interfacial Aspects of Biomedical Polymers. Plenum Press, New York
Antosiewicz J, Porschke D (1989) The nature of protein dipole moments: experimental and calculated permanent dipole of α-chymotrypsin. Biochemistry 28:10072–10078
Bae YM, Oh B-K, Lee W, Lee WH, Choi J-W (2005) Study on orientation of immunoglobulin G on protein G layer. Biosens Bioelectron 21:103–110
Bizzi M, Basini L, Saracco G, Specchia V (2002) Short contact time catalytic partial oxidation of methane: analysis of transport phenomena effects. Chem Eng J 90:97–106
Boumaza F, Dejardin P, Yan F, Bauduin F, Holl Y (1992) Fibrinogen adsorption on Pyrex glass tubes – a continuous kinetic study. Biophys Chem 42:87–92
Bowen BD, Levine S, Epstein N (1976) Fine particle deposition in laminar flow through parallel-plate and cylindrical channels. J Colloid Interface Sci 54:375–390
Bowen BD, Epstein N (1979) Fine particle deposition in smooth parallel-plate channels. J Colloid Interface Sci 72:81–97
Brash J, Horbett TA (1995) Proteins at Interfaces II: Fundamentals and Applications. American Chemical Society, Washington DC, USA
Britt DW, Buijs J, Hlady V (1998) Tobacco mosaic virus adsorption on self-assembled and Langmuir-Blodgett monolayers studied by TIRF and SFM. Thin Solid Films 329:824–828
Buijs J, Britt DW, Hlady V (1998) Human growth hormone adsorption kinetics and conformation on self-assembled monolayers. Langmuir 14:335–341
Burns TE, Dennison JR (1998) Physisorbed CO on ionic crystals: an extended BEG spin-lattice model of adsorbed dipolar molecules. Surf Sci 395:46–59
Burns TE, Dennison JR, Kite J (2004) Extended BEG model of monhalogenated methanes physisorbed on ionic crystals. Surf Sci 554:211–221
Calonder C, Van Tassel PR (2001) Kinetic regimes of protein adsorption. Langmuir 17:4392–4395
Coltrin ME, Mitchell CC (2003) Mass transport and kinetic limitations in MOCVD-selective area growth. J Cryst Growth 254:35–45
Cuypers PA, Hermens WT, Hemker HC (1978) Ellipsometry as a tool to study protein films at liquid–solid interfaces. Anal Biochem 84:56–67
Dabros T, van de Ven TGM (1993) Particle deposition on partially coated surfaces. Colloids Surf A 75:95–104
Daly SM, Przybycien TM, Tilton RD (2003) Coverage-dependent orientation of lysozyme adsorbed on silica. Langmuir 19:3848–3857
Dejardin P, Le MT, Wittmer J, Johner A (1994) Adsorption rate in the convection-diffusion model. Langmuir 10:3898–3901
Dejardin P, Vasina EN (2004) An accurate simplified data treatment for the initial adsorption kinetics in conditions of laminar convection in a slit: application to protein adsorption. Colloids Surf B 33:121–127
Docoslis A, Wu W, Giese RF, van Oss CJ (1999) Measurements of kinetic constants of protein adsorption onto silica particles. Colloids Surf B 13:83–104
Ethève J, Dejardin P (2002) Adsorption kinetics of lysozyme on silica at pH 7.4: correlation between streaming potential and adsorbed amount. Langmuir 18:1777–1785
Giacomelli CE, Norde W (2001) The adsorption-desorption cycle. Reversibility of the BSA-silica system. J Colloid Interface Sci 233:234–240
Göransson A, Trägardh C (2000) An experimental study of the kinetics of particle deposition in a wall-jet cell using total internal reflection fluorescence. J Colloid Interface Sci 231:228–237
Holmberg K, Tiberg F, Malmsten M, Brink C (1997) Grafting with hydrophilic polymer chains to prepare protein-resistant surfaces. Colloids Surf A 123–124:297–306

Hook F, Voros J, Rodahl M, Kurrat R, Boni P, Ramsden JJ, Textor M, Spencer ND, Tengvall P, Gold J, Kasemo B (2002) A comparative study of protein adsorption on titanium oxide surfaces using in situ ellipsometry, optical waveguide lightmode spectroscopy, and quartz crystal microbalance/dissipation. Colloids Surf B 24:155–170

Huang XJ, Xu ZK, Wan LS, Wang ZG, Wang JL (2005) Surface modification of polyacrylonitrile-based membranes by chemical reactions to generate phospholipid moieties. Langmuir 21:2941–2947

Hunter RJ (1981) Zeta potential in colloid science. Principles and applications. In: Ottewill RH, Rowell RL (eds) Colloid Science. Academic Press, London, p 81

Ishihara K, Fukumoto K, Iwasaki Y, Nakabayashi N (1999a) Modification of polysulfone with phospholipid polymer for improvement of the blood compatibility. Part 1. Surface characterization. Biomaterials 20:1545–1551

Ishihara K, Fukumoto K, Iwasaki Y, Nakabayashi N (1999b) Modification of polysulfone with phospholipid polymer for improvement of the blood compatibility. Part 2. Protein adsorption and platelet adhesion. Biomaterials 20:1553–1559

Iwasaki Y, Tojo Y, Kurosaki T, Nakabayashi N (2003) Reduced adhesion of blood cells to biodegradable polymers by introducing phosphorylcholine moieties. J Biomed Mater Res A 65:164–169

Kelly MS, Santore MM (1995) The role of a single end group in poly(ethylene oxide) adsorption on colloidal and film polystyrene: complimentary sedimentation and total internal reflectance fluorescence studies. Colloids Surf A 96:199–215

Kojima M, Ishihara K, Watanabe A, Nakabayashi N (1991) Interaction between phospholipids and biocompatible polymers containing a phosphorylcholine moiety. Biomaterials 12:121–124

Ladam G, Schaaf P, Decher G, Voegel J-C, Cuisinier FJG (2002) Protein adsorption onto auto-assembled polyelectrolyte films. Biomol Eng 19:273–280

Le MT, Dejardin P (1998) Simultaneous adsorption of fibrinogen and kininogen at a silica/solution interface. Langmuir 14:3356–3364

Lee J, Kopecek J, Andrade J (1989) Protein-resistant surfaces prepared by PEO-containing block copolymer surfactants. J Biomed Mater Res 23:351–368

Lee J, Kopeckova P, Kopecek J, Andrade J (1990) Surface properties of copolymers of alkyl methacrylates with methoxy(polyethyleneoxyde) methacrylates and their application as protein-resistant coatings. Biomaterials 11:455

Leonard E, Turitto V, Vroman L (1987) Blood in Contact with Natural and Artificial Surfaces. New York Academy of Sciences, New York

Lévêque M (1928) Les lois de transmission de la chaleur par convection. Faculté des Sciences, Paris

Levich VG (1962) Physical Hydrodynamics. Prentice-Hall, Englewood Cliffs, NJ, USA

Malmsten M, Lassen B, Holmberg K, Thomas V, Quash G (1996) Effects of hydrophilization and immobilization on the interfacial behavior of immunoglobulins. J Colloid Interface Sci 177:70–78

Mar MN, Ratner BD, Yee SS (1999) An intrinsically protein-resistant surface plasmon resonance biosensor based upon a RF-plasma-deposited thin film. Sens Actuators B 54:125–131

McClellan SJ, Franses EI (2005) Adsorption of bovine serum albumin at solid/aqueous interfaces. Colloids Surf 260:265–275

Nakabayashi N, Williams DF (2003) Preparation of non-thrombogenic materials using 2-methacryloyloxyethyl phosphorylcholine. Biomaterials 24:2431–2435

Nakabayashi N, Iwasaki Y (2004) Copolymers of 2-methacryloyloxyethyl phosphorylcholine (MPC) as biomaterials. Bio-Med Mater Eng 14:345–354

Nitschke M, Menning A, Werner C (2000) Immobilization of PEO-PPO-PEO triblock copolymers on PTFE-like fluorocarbon surfaces. J Biomed Mater Res 50:340–343

Noinville S, Revault M, Baron M-H (2002a) Conformational changes of enzymes adsorbed at liquid–solid interface: relevance to enzymatic activity. Biopolymers 67:323–326

Noinville S, Revault M, Baron M-H, Tiss A, Yapoudjian S, Ivanova M, Verger R (2002b) Conformational changes and orientation of Humicola lanuginosa lipase on a solid hydrophobic surface: an in situ interface Fourier transform infrared–attenuated total reflection study. Biophys J 82:2709–2719

Noinville S, Bruston F, El Amri C, Baron D, Nicolas P (2003) Conformation, orientation, and adsorption kinetics of dermaseptin B2 onto synthetic supports at aqueous/solid interface. Biophys J 85:1196–1206

Norde W, Rouwendal E (1990) Streaming potential measurements as a tool to study protein adsorption kinetics. J Colloid Interface Sci 139:169–176

Norde W, Zoungrana T (1998) Surface-induced changes in the structure and activity of enzymes physically immobilized at solid/liquid interfaces. Biotechnol Appl Biochem 28:133–143

Poksinski M, Arwin H (2004) Protein monolayers monitored by internal reflection ellipsometry. Thin Solid Films 455–456:716–721

Price ME, Cornelius RM, Brash JL (2001) Protein adsorption to polyethylene glycol modified liposomes from fibrinogen solution and from plasma. Biochim Biophys Acta 1512:191–205

Quiquampoix H, Ratcliffe RG (1992) A P-31 NMR Study of the adsorption of bovine serum albumin on montmorillonite using phosphate and the paramagnetic cation Mn^{2+}-modification of conformation with pH. J Colloid Interface Sci 148:343–352

Ramsden JJ, Lvov YM, Decher G (1995) Determination of optical constants of molecular films assembled via alternate polyion adsorption. Thin Solid Films 254:246–251

Rebar VA, Santore MM (1996) History-dependent isotherms and TIRF calibrations for homopolymer adsorption. Macromolecules 29:6262–6272

Robeson JL, Tilton RD (1996) Spontaneous reconfiguration of adsorbed lysozyme layers observed by total internal reflection fluorescence with a pH-sensitive fluorophore. Langmuir 12:6104–6113

Schaaf P, Dejardin P (1988) Structural changes within an adsorbed fibrinogen layer during the adsorption process: a study by scanning angle reflectometry. Colloids Surf 31:89–103

Seitz R, Brings R, Geiger R (2005) Protein adsorption on solid–liquid interfaces monitored by laser ellipsometry. Appl Surf Sci 252:154–157

Servagent-Noinville S, Revault M, Quiquampoix H, Baron MH (2000) Conformational changes of bovine serum albumin induced by adsorption on different clay surfaces: FTIR analysis. J Colloid Interface Sci 221:273–283

Su TJ, Lu JR, Thomas RK, Cui ZF, Penfold J (1998) The effect of solution pH on the structure of lysozyme layers adsorbed at the silica–water interface studied by neutron reflection. Langmuir 14:438–445

Tirelli N, Lutolf MP, Napoli A, Hubbell JA (2002) Poly(ethylene glycol) block copolymers. Rev Mol Biotechnol 90:3–15

Ueda T, Watanabe A, Ishihara K, Nakabayashi N (1991) Protein adsorption on biomedical polymers with a phosphorylcholine moiety adsorbed with phospholipid. J Biomater Sci Polym Ed 3:185–194

Valette P, Thomas M, Dejardin P (1999) Adsorption of low molecular weight proteins to hemodialysis membranes: experimental results and simulations. Biomaterials 20:1621–1634

Vasina EN, Dejardin P (2004) Adsorption of alpha-chymotrypsin onto mica in laminar flow conditions. Adsorption kinetic constant as a function of tris buffer concentration at pH 8.6. Langmuir 20:8699–8706

Vasina EN, Dejardin P, Rezaei H, Grosclaude J, Quiquampoix H (2005) Fate of prions in soil: adsorption kinetics of recombinant unglycosylated ovine prion protein onto mica in laminar flow conditions and subsequent desorption. Biomacromolecules 6:3425–3432

Vermeer AWP, Norde W (2000) The influence of the binding of low molecular weight surfactants on the thermal stability and secondary structure of IgG. Colloids Surf A 161:139–150

Vermeer AWP, Giacomelli CE, Norde W (2001) Adsorption of IgG onto hydrophobic Teflon. Differences between the Fab and Fc domains. Biochim Biophys Acta 1526:61–69

Voegel JC, Dejardin P, Strasser C, de Baillou N, Schmitt A (1987) Thermal desorption spectrometry of fibrinogen. Colloids Surf 25:139–144

Werner C, Eichhorn KJ, Grundke K, Simon F, Grahlert W, Jacobasch HJ (1999) Insights on structural variations of protein adsorption layers on hydrophobic fluorohydrocarbon polymers gained by spectroscopic ellipsometry (part I). Colloid Surf A 156:3–17

Wertz CF, Santore MM (1999) Adsorption and relaxation kinetics of albumin and fibrinogen on hydrophobic surfaces: single species and competitive behavior. Langmuir 15:8884–8894

Wertz CF, Santore MM (2002) Adsorption and reorientation kinetics of lysozyme on hydrophobic surfaces. Langmuir 18:1190–1199

Wu YJ, Timmons RB, Jen JS, Molock FE (2000) Non-fouling surfaces produced by gas phase pulsed plasma polymerization of an ultra low molecular weight ethylene oxide containing monomer. Colloids Surf B 18:235–248

Xu Z, Marchant RE (2000) Adsorption of plasma proteins on polyethylene oxide-modified lipid bilayers studied by total internal reflection fluorescence. Biomaterials 21:1075–1083

Yan F, Dejardin P, Mulvihill JN, Cazenave JP, Crost T, Thomas M, Pusineri C (1992) Influence of a preadsorbed terpolymer on human platelet accumulation, fibrinogen adsorption, and ex vivo blood activation in hemodialysis hollow fibers. J Biomater Sci Polym Ed 3:389–402

Ye SH, Watanabe J, Iwasaki Y, Ishihara K (2005) In situ modification on cellulose acetate hollow fiber membrane modified with phospholipid polymer for biomedical application. J Membr Sci 249:133–141

Zembala M, Dejardin P (1994) Streaming potential measurements related to fibrinogen adsorption onto silica capillaries. Colloids Surf B 3:119

Zembala M, Adamczyk Z (2000) Measurements of streaming potential for mica covered by colloid particles. Langmuir 16:1593–1601

Zembala M, Adamczyk Z, Warszynski P (2001) Influence of adsorbed particles on streaming potential of mica. Colloids Surf A 195:3–15

Zembala M (2004) Electrokinetics of heterogeneous interfaces. Adv Colloid Interface Sci 112:59–92

Zoungrana T, Findenegg GH, Norde W (1997) Structure, stability, and activity of adsorbed enzymes. J Colloid Interface Sci 190:437–448